

1 **NO₂ seasonal evolution in the North Subtropical free** 2 **troposphere**

3

4 **M. Gil-Ojeda¹, M. Navarro-Comas¹, L. Gómez-Martín¹, J.A. Adame¹, A. Saiz-**
5 **Lopez², C. A. Cuevas², Y. González³, O. Puentedura¹, E. Cuevas³, J-F**
6 **Lamarque⁴, D. Kinninson⁴ and S. Tilmes⁴**

7 [1]{Instituto Nacional de Técnica Aeroespacial, Torrejón de Ardoz, Spain }

8 [2]{Atmospheric Chemistry and Climate Group, Institute of Physical Chemistry Rocasolano,
9 CSIC, Madrid, Spain }

10 [3]{Izaña Atmospheric Research Center, AEMET, Tenerife, Spain }

11 [4]{Atmospheric Chemistry Division, NCAR, Boulder, CO, USA }

12 Correspondence to: M. Gil-Ojeda (gilm@inta.es)

13

14 **Abstract**

15 Three years of Multi-Axis Differential Optical Absorption Spectroscopy (MAXDOAS)
16 measurements (2011-2013) have been used for estimating the NO₂ mixing ratio along a
17 horizontal line of sight from the high mountain Subtropical observatory of Izaña, at 2370 m
18 a.s.l. (NDACC station, 28.3°N, 16.5°W). The method is based on horizontal path calculation
19 from the O₂-O₂ collisional complex at the 477 nm absorption band which is measured
20 simultaneously to the NO₂, and is applicable under low aerosols loading conditions.

21 The MAXDOAS technique, applied in horizontal mode in the free troposphere, minimizes the
22 impact of the NO₂ contamination resulting from the arrival of MBL airmasses from thermally
23 forced upwelling breeze during central hours of the day. Comparisons with in situ
24 observations show that during most of measuring period the MAXDOAS is insensitive or
25 very little sensitive to the upwelling breeze. Exceptions are found under pollution events
26 during southern wind conditions. On these occasions, evidence of fast efficient and
27 irreversible transport from the surface to the free troposphere is found.

28 Background NO₂ vmr, representative of the remote free troposphere, are in the range of 20-45
29 pptv. The observed seasonal evolution shows an annual wave where the peak is in phase with

1 the solar radiation. Model simulations with the chemistry-climate CAM-Chem model are in
2 good agreement with the NO₂ measurements, and are used to further investigate the possible
3 drivers of the NO₂ seasonality observed at Izaña.

4 5 **1 Introduction**

6 Nitrogen oxides play an important role in tropospheric chemistry as they control the O₃
7 photochemical catalytic production (Crutzen, 1979), the abundance of hydroxyl radicals, and
8 contribute to the nitrate aerosols formation. In a background unpolluted atmosphere where
9 NO_x concentrations are low, net ozone loss occurs during photochemically active periods (Liu
10 et al., 1983; Isaksen et al., 2005). NO_x abundance is highly variable since it is influenced by
11 non-steady natural and anthropogenic emissions and its global distribution is still uncertain.
12 Free Troposphere (FT) source inventories indicate that major production comes from lightning
13 (2-16 Tg N yr⁻¹), followed by NH₃ oxidation (0.3-3 Tg N yr⁻¹), stratospheric intrusion (0.08-1
14 Tg N yr⁻¹) and aircraft (0.6-0.7 Tg N yr⁻¹). Contribution from the boundary layer in remote
15 regions is rare (Bradshaw et al., 2000).

16 Information of surface NO_x on polluted areas is available due to extended governmental air
17 quality networks. During the last decade, satellite instruments have demonstrated capabilities
18 for successful retrieval of tropospheric NO₂ identifying enhanced concentrations over urban
19 and industrial areas in the boundary layer (Richter et al., 2005; Irie et al., 2005) and tracking
20 the temporal trends (Hilboll et al., 2013; Cuevas et al., 2014). However, direct NO₂
21 measurements in the background FT are scarce due to the requirement of observational
22 platforms above, typically 2000 m a.s.l., but also due to the low concentrations present at
23 those levels.

24 Airborne NO₂ measurements have been performed for decades (Ridley et al., 1988; Carroll et
25 al., 1990), however the need for very short response times at concentrations close to the
26 instrumental detection limit, make the FT observations a challenging task. Even though well
27 characterized aircraft instruments reach detection limits as low as 10 pptv (Heland et al.,
28 2002), few studies are reported in the literature. Measurements are generally collected during
29 individual field campaigns associated to specific targets such as chemistry missions or
30 satellite validations (Jacob et al., 2003; Bucsela et al., 2008; Boersma et al., 2008; Baidar et
31 al., 2013; Flynn et al., 2014). These time and space sparse data limit the study of seasonalities
32 or trends in the FT. Only recently, attempts to obtain global FT NO₂ abundances from satellite

1 OMI instrument has been performed for the first time (Choi et al., 2014) by using the cloud
2 slicing technique (Ziemke 2001). The method is based on the comparison of cloud and
3 cloudless scenes to derive the FT mean concentrations. Results show that valuable
4 information on NO₂ large scale phenomena can be derived on areas where clouds presence is
5 frequent but does not provide results in places such as East Atlantic subtropical latitudes
6 where high pressures are dominant features.

7 Instruments operating in the few high mountain stations existent around the world are the only
8 alternative to monitor NO₂ in the background FT. However, the in situ measurements are
9 often affected by the “upslope breeze effect” (Kleissl et al., 2007; Val Martin et al., 2008;
10 Rodriguez et al., 2009; Reidmiller et al., 2010; Cuevas et al., 2013). Radiative heating in the
11 mountain slopes result in air upwelling from the boundary layer contaminating the daytime
12 measurements by generally larger values over the polluted lower layers.

13 Recently, Gomez et al. (2014) have presented a simple method based on a Modified
14 Geometrical Approximation (MGA) to estimate trace gases concentrations at the level of the
15 Izaña Observatory from MAXDOAS measurements. The horizontal path length is obtained
16 from the oxygen collisional complex (O₄, hereafter) simultaneously measured with the tracer
17 under consideration (NO₂ and O₃). Gomez et al. examined a short summer period to
18 demonstrate the validity of the method. Here we apply the same technique to data covering 3
19 full years (2011-2013) to analyze the seasonal evolution of the NO₂ concentrations in volume
20 mixing ratio (vmr). MAXDOAS present two main advantages with respect to the in situ
21 instrument at this location, both related to the very long optical path of the measurements of
22 over 60 km. Firstly, it minimizes the potential contribution of NO₂ that may be upwelled from
23 the marine boundary layer (MBL). The breeze layer has a limited vertical extension and its
24 relative contribution to the MAXDOAS long path is small. On the contrary, Izaña in situ data
25 around noon are strongly influenced by the underlying polluted MBL (Puentedura et al.,
26 2012; Gomez et al., 2014). Secondly, due to the long light paths achieved by MAXDOAS in
27 the FT, very low concentrations, of few ppt, can be measured.

28 Section 2 presents the method, limits and associated errors. In Sect. 3 the station and data sets
29 are depicted. Section 4 describes the method used for profiles retrieval. The description of the
30 chemical and back trajectories models is done in Sect. 5. Finally, Sects. 6 and 7 present the
31 results and discussion, and summary, respectively.

32

2 Instrument and methodology

In year 2010 the DOAS spectrometer, operating in zenith mode at that time, was upgraded for MAXDOAS measurements. The spectrometer records the sky spectrum in the visible range at a spectral resolution of 0.55 nm in 10 elevation angles from -1 to 90°, and 1° field of view covering a full cycle in 20 min. The number of cycles per day ranges from 26 at winter solstice to 38 in summer. NO₂ is evaluated in the 425-520 nm range in order to simultaneously retrieve the O₄ from the 477 nm absorbing band. The scanning plane is on 0° azimuth (North) to minimize the dependence of the path with the azimuth (Wittrock et al., 2004). The instrument is part of the Network for the Detection of the Atmospheric Composition Change (NDACC) and other settings are those recommended for DOAS type spectrometers. NO₂ at 294K temperature from Vandaele et al. (1998) and O₄ from Hermans et al. (1990) cross sections have been used. Details of the instrument, settings and operational mode can be found in Puentedura et al. (2012) and Gomez et al. (2014).

The Modified Geometry Approximation (MGA) described in Gomez et al., (2014) has been used for the data analysis. NO₂ vmr at the level of the station is obtained by dividing the differential slant column density (DSCD) measured in the horizontal geometry by the horizontal optical path. The DSCD is obtained by subtracting the measurement obtained at the zenith (SZA=90°) from the measurement in the horizontal path. In a first approximation, the slant paths contributions of 0 and 90° geometries cancel out and only the signal of the tracers present in the horizontal path remains (See Gomez et al., 2014 for details). The method assumes a quasi-Rayleigh atmosphere, i.e. very low Aerosol Optical Depth (AOD), and a single scattering before the photon reaches the detector. The path is obtained from the O₄ horizontal column since the amount of O₂ is known from the independent air pressure measurements. The path length is then corrected to account for the differences in wavelengths between the O₄ and NO₂ analysis ranges. In practice, the scattering of the zenith path does not take place near the instrument but at a few km above the level of the station. The actual concentration of a measured species X at the station level is given by:

$$X_{vmr} = \frac{X_{DSCD}}{\frac{O_{4DSCD}}{[O_4]_{surface}} \cdot f + c} \quad [1]$$

1

2 Where X_{DSCD} and O_{4DSCD} are the slant measured columns of the species X and O_4 ,
3 respectively. $[O_4]_{surface}$ is the O_4 at the level of the station, f is the correction factor due to
4 differences in wavelength absorption ranges of the specie under study with respect to O_4 that
5 can be computed from a radiative transfer model (RTM) and c is the error of the approach.
6 The latter is a factor accounting for the dependence with the different vertical distributions of
7 both species and AMFs.

8

$$9 \quad c = h(Rg - R' g') \quad [2]$$

10

11 h is the effective scattering height of the vertical ray. R and R' are the ratio of the mean
12 concentration of the layer divided by the concentration at the level of the station of tracer X
13 and O_4 , respectively, and g and g' accounts for their AMF in the zenith geometry
14 ($g=AMF(SZA)-1$), where SZA stands for Solar Zenith Angle.

15 The effective scattering height is defined as

$$16 \quad h(z) = \sum_{surface}^{top} \left(\frac{I(z)}{\int_{surface}^{top} I(z).dz} .z \right) \quad [3]$$

18

19

$$20 \quad \text{where } \frac{I(z)}{\int_{surface}^{top} I(z).dz}$$

21

22 represents the normalized contribution of the ray scattered at each atmospheric layer to the
23 total flux at surface. From radiative transfer calculations it can be shown that the effective
24 scattering height ranges between 6.5 and 7.5 km above the station for solar zenith angle
25 (SZA) below 70° , which we estimate as the validity limit of the method.

26 Since both NO_2 and O_4 are analyzed in the same spectral range, the difference between the
27 weighted center of the range for NO_2 , i.e. the effective wavelength, and that of O_4 is small.
28 The value of f is of 0.9 for a near-Rayleigh atmosphere.

1 By using Eq. (2), the error introduced in NO₂ vmr due to the geometrical approximation, if
2 assuming a constant mixing ratio of both O₄ and NO₂ with height, is of 9.0 % at 70° SZA and
3 of 2.3% at 50°. Since the scattering heights and the air mass factors are well known, the data
4 can be corrected. The only uncertainty is due to the R value related to the vertical distribution
5 of NO₂ within the FT. However, aircraft measurements over the ocean far from large
6 industrial areas show that the tropospheric vertical distribution is nearly constant above the
7 MBL (Bucsela et al., 2008)

8 In the presence of moderate or high aerosols loading at the level of the observational point,
9 multiple scattering takes place and the method is no longer valid. Assuming that the aerosol
10 layer is a well mixed layer, we estimate the AOD=0.1 at 500 nm as a safe limit (Gomez et al.,
11 2014).

12 Since the path length is obtained from O₄ measurements, uncertainty in the magnitude of its
13 absolute cross section is an additional source of error. It has been reported that paths obtained
14 from O₄ are even larger than that RT computed for a Rayleigh atmosphere (Wagner et al.,
15 2002) when using the generally accepted cross-sections reported in literature (Greenblatt,
16 1990; Hermans et al., 1999), suggesting that cross-section are underestimated. There is,
17 however, no agreement in the magnitude of the correct values. We performed direct Sun
18 measurements on a very clear morning (Aerosol Optical Density at 500 nm over the
19 observatory = 0.007 ± 0.00077) at an O₄ effective temperature of 250 K, and compared the
20 retrieved slants columns with the ones calculated from the local radiosounding of the day (7
21 October, 2014) up to 30 km and the tropical standard atmosphere from 30 km upwards.
22 Results show an excellent agreement with no difference at the error level when the retrieval
23 includes O₄ cross-sections at two temperatures (Fig. 1). In this exercise, the Thalman &
24 Volkamer (2013) cross-sections at 203 and 293 K were used. When including only the room
25 temperature cross-section in the retrieval, the obtained O₄ is 3-5 % too large.

26 Our results agree with the very recent report by Spinei et al. (2014) who found a temperature
27 dependence of 9% for a variation of 44 K and no pressure dependence based on direct sun and
28 aircraft MAXDOAS measurements. The conclusion of their work is that no corrections need
29 to be made for effective temperatures near 275 K. Since the present method uses only the
30 horizontal path, the temperature along the path is nearly constant and the seasonal variability
31 in the subtropical FT is small. Air temperature at the level of Izaña ranges from 277 K in

1 January-February to 287 K in July-August. Consequently, no more than 2 % of error is
2 expected due to this effect.

3 Typical NO₂ SCD root mean square error of the fit for horizontal geometry is of 3×10^{14}
4 molec cm⁻². These errors represent 15–20 % of the typical differential SCD. A summary of
5 the analysis errors is shown in Table 1.

6

7 **3 The Izaña observatory and dataset**

8

9 Izaña (28.3°N, 16.5°W) is a well known GAW-NDACC station located at the top of the Izaña
10 mountain, one of the peaks of the great crater of the Teide volcano, at 2370 m a.s.l., in
11 Tenerife Island. The observatory and related meteorology has been extensively described in
12 previous publications (i.e. Rodriguez et al., 2009; Cuevas et al., 2013). It is representative of
13 the FT at night. During daytime it is frequently affected by anabatic winds resulting from
14 heating of the ground. This upslope breeze carries boundary layer air masses to the FT. The
15 intensity of the wind peaks near the local noon and can extend well into the afternoon. It can
16 be indirectly quantified using the measurements of water vapour on the station since air
17 masses from below carry high humidity to the height of the observatory. The measurements
18 of in situ NO₂ are also useful for this purpose, since the BL NO₂ concentrations in populated
19 areas near the coast are typically more than one order of magnitude larger than the
20 background FT.

21 For the present work only the horizontal spectra are analyzed. If the SZA was lower than 10°,
22 then the 70° elevation spectrum was used as reference to avoid spectral distortions due to too
23 short integration times. In all other cases the reference was the zenith spectrum of the same
24 cycle.

25 Data from three complete years (2011-2013) have been used after screening for (a) NO₂
26 RMSE: Fit error is limited to 2×10^{15} molec cm⁻² and a signal to noise ratio of 0.5, which is
27 approximately the detection limit of the instrument. (b) High SZA: Only data corresponding
28 to data below SZA 70° are used in the present analysis to limit the error in the path
29 calculations. (c) Aerosol loading: Measurements on days with Aerosol Optical Depth (AOD)
30 at 500 nm over 0.1, were rejected. (d) Length of the path: Individual measurements with paths
31 shorter than 30 km were also rejected (broken clouds or narrow dust layers might cause this

1 effect). (e) Unrealistic negative values appearing occasionally. Over 15.000 of data passed all
2 filters for the 3 years period (40% of all possible data).

3

4 **4 The Optimal Estimation Method**

5 The Optical Estimation Method (OEM) has been extensively used on last years to obtain NO₂
6 vertical profiles on moderate to high polluted environments. However, on free troposphere
7 background conditions, the concentrations are near the instrumental detection limit (10-100
8 pptv) and in these conditions the method provide unrealistic profiles. In this work we have
9 used it only to characterize the vertical distribution of the plume in a particular case study in
10 which a high NO₂ airmass arrived to the station. The mean AOD-500 nm on the studied day
11 was of only 0.02. Consequently aerosols have not been included in the analysis.

12 Given a set of measurements \mathbf{y} with the errors covariance \mathbf{S}_ϵ , the OEM (Rodgers, 2000)
13 provides the state vector \mathbf{x} that maximizes the probability that \mathbf{x} , containing the trace gas
14 vertical distribution, belongs to the interval $[\mathbf{x}, \mathbf{x}+d\mathbf{x}]$. Following OEM approach, the
15 maximum a posteriori solution $\hat{\mathbf{x}}$ is calculated as:

$$16 \quad \hat{\mathbf{x}} = \mathbf{x}_a + \mathbf{S}_a \mathbf{K}^T (\mathbf{K} \mathbf{S}_a \mathbf{K}^T + \mathbf{S}_\epsilon)^{-1} (\mathbf{y} - \mathbf{K} \mathbf{x}_a) = \mathbf{x}_a + \mathbf{G}_y (\mathbf{y} - \mathbf{K} \mathbf{x}_a)$$

17 Where the weighting functions matrix \mathbf{K} express the sensitivity of the measurements to
18 variations in the trace gas profile (NO₂ in this case). In this work, \mathbf{K} is obtained with the
19 SPSPDISORT pseudo-spherical radiative transfer solver of the libRadtran software package
20 (Mayer and Kylling, 2005). The \mathbf{x}_a vector and \mathbf{S}_a matrix correspond to an a priori NO₂ profile
21 and its corresponding error covariance matrix, respectively.

22 The gain matrix \mathbf{G}_y , given by the following expression, quantifies the sensitivity of the
23 retrieval to the measurements:

$$24 \quad \mathbf{G}_y = \mathbf{S}_a \mathbf{K}^T (\mathbf{K} \mathbf{S}_a \mathbf{K}^T + \mathbf{S}_\epsilon)^{-1}$$

25 The averaging kernel matrix \mathbf{A} , is then obtained as follows:

$$26 \quad \mathbf{A} = \mathbf{G}_y \mathbf{K}$$

1 **A** expresses the sensitivity of the retrieval to the true state, and it has an important role in the
 2 characterization of the retrieval. The retrieval at a given altitude is an average of the total
 3 profile weighted by the corresponding row of **A**, also known as Averaging Kernel function
 4 (AK). In general, the AKs are functions with a single peak in the appropriate level, where the
 5 measurement provides additional information to add to the a priori profile. Trace of **A**
 6 provides the independent pieces of information that can be extracted from the retrieval,
 7 usually known as degrees of freedom (DFS).

8 Another parameter that determines the quality of the retrievals is the total error of the state
 9 vector elements. This parameter is the addition of three contributions: (1) the smoothing of
 10 the true profiles given by **S_a**; (2) The systematic errors of the measurements, provided by **S_ε**;
 11 and (3) systematic errors of the forward model mainly provided by the uncertainties in the
 12 parameters characterizing the atmosphere. The choose of the values corresponding to these
 13 three sources of error (**S_a**, **S_ε** and the atmosphere parameters) in our study will be described in
 14 the following paragraphs.

15 The NO₂ hourly profiles used as a priori profiles in our calculations were obtained using a
 16 photochemical box model (Denis et al., 2005) derived from the SLIMCAT 3-D chemical
 17 transport model (Chipperfield, 2006). Diagonal elements of **S_a** are usually chosen to be a
 18 percentage of **x_a**. In this case, following the L-curve method described in (Schofield, 2003),
 19 they have been set to 100% of **x_a**, and its non-diagonal elements are calculated as follows
 20 (Barret et al., 2002; Friess et al., 2006):

$$21 \quad S_{aij} = \sqrt{S_{a ii} S_{a jj} \exp(-\ln 2) \left(\frac{(z_i - z_j)^2}{\gamma^2} \right)}$$

22 Where z_i and z_j are the altitudes of the altitude grid levels i and j respectively, and γ is a half
 23 of the correlation length. The functions represented in the last equation are Gaussian
 24 correlation functions which account for correlations between trace gas concentrations at
 25 different altitudes. After several tests on the retrieval, γ value has been chosen to be 300 m,
 26 correspondings to the value (between 0.1 and 1 km) that maximizes the DFS (trace of **A**), for
 27 the overall retrieval as well as for the altitudes closer to the station (2.3-2.6 km).

28 In this work, **y** represents the differential slant column densities (DSCD) of NO₂ measured
 29 with the MAX-DOAS spectrometer, and **S_ε** is set to a diagonal matrix which diagonal
 30 elements correspond to the molecular errors of the measurements.

1 Concerning parameters characterizing atmosphere in our calculations, vertical profiles of O₃,
2 O₂, CO₂ and H₂O have been obtained from the standard atmosphere for tropical latitudes
3 (Anderson, 1986). Radio-sounding data performed the same day of our calculations provided
4 the pressure, temperature and air density vertical profiles used in our retrieval. We have
5 considered layers of 100 m from 0 to 10 km, and with the same width of those corresponding
6 to the standard atmosphere for tropical latitudes (Anderson, 1986) for altitudes over 10 km. In
7 this work, AKs are near zero for altitudes lower than 0.5 km and higher than 5 km. The
8 retrieved profiles have been obtained for altitudes up to 6 km.

9

10 **5 Model description and trajectory analysis**

11 CAM-Chem (Community Atmosphere Model with Chemistry) is a global 3D chemistry-
12 climate model fully integrated into the CESM framework (Community Earth System Model)
13 (Lamarque et al., 2012). In this work CAM-Chem has been configured using a horizontal grid
14 resolution of 1.91 latitude × 2.5° longitude and 26 hybrid vertical levels from the surface to
15 approximately 38 km. All simulations have been performed in Specified dynamics (SD),
16 using offline meteorological fields to compute the atmospheric transport, considering the
17 same high frequency meteorological input from a previous CAM-Chem 15 years simulation.
18 This implies that the model is forced to evolve as if it were a Chemical Transport Model.

19 The model includes the tropospheric chemistry mechanism of MOZART-4 (Emmons et al.,
20 2010), implementing also organic and inorganic halogen (chlorine, bromine and iodine)
21 photochemistry mechanism, taking into account natural and anthropogenic sources,
22 heterogeneous recycling and dry and wet deposition (Saiz-Lopez et al., 2012; Ordoñez et al.,
23 2012; Fernandez et al., 2014). Anthropogenic emissions due to fossil fuel and biofuel
24 combustions come from the POET (Precursors of Ozone and their effects in the troposphere)
25 database for 2000 (Granier et al., 2005).

26 To investigate the air masses reaching the area of study, back trajectories were computed
27 with the HYSPLIT (Hybrid Single-Particle Lagrangian Integrated Trajectory) model,
28 developed by the NOAA's Air Resources Laboratory (ARL) (Draxler et al., 2009). The
29 ECMWF (European Centre for Medium Range Weather Forecasts) meteorological fields were
30 used with a spatial resolution of 0.25°x0.25°, 22 vertical levels from the surface to 250 mb
31 and a time resolution of 6 h. Three-dimensional kinematic back trajectories were calculated. A
32 daily back-trajectory at 12:00 UTC, with a 168 h pathway (7 days) and at 2370 m a.s.l. was

1 computed. Following the HYSPLIT model tools back trajectories have been grouped in
2 clusters (Stunder, 1996), arriving at the Izaña observatory.

3

4 **6 Results and discussion**

5 **6.1 MAXDOAS vs. in situ**

6 Results of the NO₂ comparison can be classified according to three different meteorological
7 regimes. A period in 2013 has been selected to illustrate the differences in concentration
8 between the in situ local sampling and the MAXDOAS long-path average (Fig. 2, upper
9 panel). On days when the breeze is inhibited, the in situ data are representative of the FT, and
10 the agreement between instruments is very good (e.g. days 139-145). On days when anabatic
11 winds are present, NO₂ vmr increases are observed in the in situ measurements whereas
12 MAXDOAS signal remains at typical FT levels (e.g. days 130-137). Upslope winds cause an
13 air mass mixture with that associated by the FT synoptic wind. The upslope strength will
14 depend inversely on the intensity of the zonal synoptic winds. (Cuevas et al., 2013). In
15 general, the depth of the layer is not enough to contaminate the MAXDOAS path. This
16 situation is the one most commonly observed at Izaña. As expected, MAXDOAS provide a
17 much better representation of the FT background reactive gases. A third set of measurements
18 is shown when MAXDOAS data also suffer large increases (e.g. days 127-129). After
19 excluding thunderstorms with electric activity and wildfires in the area, it was found that this
20 situation always takes place in presence of southern winds. The only identified NO₂ large
21 source upwind is the 980 MW thermal power plant located 25 km south of Izaña, with a NO₂
22 emissions of 4.7×10^6 kg year⁻¹. As previously reported (Persson and Grazzini, 2007), the
23 thermal local circulations are not captured by atmospheric global models even by the
24 ECMWF 0.25° x 0.25° used in this study which predicted trajectories above 2000 m all the
25 way (Fig. 2, lower right). This orographically-forced lifting mechanism has been found to be
26 an efficient and fast way for irreversible transport of surface air to the FT. Pollutants and
27 minor gases of oceanic origin (i.e. IO, BrO) move upslope crossing the MBL top in less than
28 1 h, and then are subsequently mixed with FT air. The quantification of the amount of air
29 mass transported from the lower layers of the MBL to the FT is out of the scope of this work,
30 but certainly data provide evidence for the existence of an efficient and fast mechanism to
31 supply halogens and other marine trace gases to the FT. Since southern wind conditions are
32 common during the summer months (50 % of the days) and the mountain rift has a NE-SW

1 orientation, and a length of about 30 km, the supply of marine trace gases to the FT might be
2 not negligible, at least on a local scale.

3 Surprisingly, the very high MAXDOAS vmr reach as much as a half of the levels observed by
4 the in situ sensor. This is related to the pointing direction of the DOAS spectrometer, since the
5 plume propagates northward, along the same direction of the spectrometer line of sight. The
6 path within the plume results in an enhancement of the absorption signal. Figure 3 shows the
7 NO₂ vmr vertical cross sections for the day 128/2013, obtained by using the OEM technique,
8 indicating that the enhancement takes place near the level of the station, with an upper limit
9 around 4 km. This confirms that once the air mass passes over the mountain obstacle it either
10 moves horizontally or descends again but remaining in the FT. Note that the instrument
11 scanning lowest angle is below the horizon (IEA = -1°), thus containing information about the
12 trace gas concentration below the station.

13 It is worth to mention that Southern winds are generally related to African air masses
14 containing Saharan dust and, as previously mentioned, those dusty days were filtered out from
15 the analysis. The only non-dusty south wind cases observed are from Atlantic air masses
16 which suffered an abrupt change in direction when approaching to Africa. Consequently the
17 impact of this effect on the overall dataset is small. Only five clear cases have been identified
18 within the 3-year record. Those cases have been removed for seasonal evolution studies.

19 Figure 4 (top panel) shows the NO₂ vmr seasonal evolution separated by year. The seasonal
20 behavior is similar in all three years, with the maximum in the summer months and the
21 minimum in winter time. Summer gaps result from the large number of Saharan dust
22 intrusions during these months. To explore a possible dependence of the retrieved
23 concentrations with the SZA, the data have been plotted in colors according the SZA (Fig. 4,
24 mid panel). The maxima in summer months are observed regardless the SZA excluding the
25 possibility of stratospheric contamination or any other SZA dependent artifact. The
26 magnitudes of the retrieved concentration are also independent of the RMSE (Fig. 4, lower
27 panel). Sporadic peaks over 100 pptv are observed with no increase in typical retrieval errors.
28 The scattering along the day is also large with standard deviations of 10-15 pptv.

29 Monthly means clearly show the rapid spring build-up and the autumn decay (Fig. 5). Mean
30 values range from 20 to 44 pptv throughout the year. A summer maximum has previously
31 been found in unpolluted continental China in the boundary layer as result of soil biogenic
32 NO emissions (Van der A et al., 2006, Qi et al., 2014). However, NO₂ in long paths over the

1 Atlantic FT cannot be explained in this way. The output of the CAM-Chem model for the
2 location and the level of the station show similar results. The agreement with observational
3 data is particularly good for the period November to February. The NO₂ summer build-up
4 takes place across the entire FT (not shown). The winter to summer ratio is largest in the
5 middle troposphere at 8 km height. The peak FT NO₂ values occurring in summer was
6 previously observed by Val-Martin et al (2008), who attributed the summer maxima in NO₂ to
7 North American biomass burning during this season. The model results show no seasonal
8 differences in the NO₂ chemical formation/loss channels. However, an increase in the overall
9 reactive nitrogen budget occurs in this unpolluted FT site, as summer proceeds. We have
10 explored two possibilities to explain the seasonality of our observations:

11 **6.1.1 Contamination by anabatic winds**

12 It has been previously shown that MAXDOAS-MGA technique minimizes the unwanted
13 effects of MBL on FT measurements, but in principle, the influence of a potential seasonal
14 cycle in the intensity of the upwelling wind cannot be entirely ruled out. Since anabatic winds
15 are driven locally by surface heating, the depth of the layer of influence is expected to be of
16 only a few hundreds of meters but there is not enough information to quantify the size of this
17 depth and thus the potential contribution of a possible path contamination from air masses
18 rich in NO₂ coming from below. Most of the works available in the literature refer to the BL,
19 generally with return flow back. However, cases of upwelling to the FT are reported as well.
20 As early as 1923, Wenger (1923) observed this situation at the slopes of the Teide mountain
21 in Tenerife to up of 1500 m a.s.l. but no data were available above that height. In situ data in
22 Fig. 1 show evidence of MBL nitrogen oxides transported by anabatic winds up to the level of
23 the station (2370 m a.s.l.). However, an intensification of the upslope breeze in summer with
24 respect to winter would result in a larger vertical extension of the upwelling layer, increasing
25 its relative contribution in the MAXDOAS path. Out of the few large pollution cases, the
26 concentrations measured are too low for the OEM technique to be applied. It is nevertheless
27 unlikely that the summer increase in upwelling can account for the twofold increase in the
28 background NO₂ vmr. For instance, for a layer of 200 m with a NO₂ load of as high as 600 ppt
29 would represent an increase in the column of some 5-10 % of the background concentration
30 for a clean day.

31 We have recalculated NO₂ monthly means only from the first morning data, namely data
32 between SZA 70° a.m. and 65° a.m. These SZA correspond to fractional days ranging from

1 0.42 in mid winter to 0.32 in summer. At this early time of day the anabatic wind is still under
2 the first stage of development and the intensity of the upwelling is of only a few percent of the
3 maximum value after noon. Results show that the seasonality in the SZA 65° to 70° data is
4 almost identical than that when considering data at all SZA (ratio >0.98). We therefore
5 conclude that the summer increase is not a result of the contamination by high NO₂ upwelled
6 MBL air masses.

7

8 **6.1.2 Changes in horizontal transport patterns along season**

9 Val-Martin et al. (2008) analysed NO₂ mountain data from Azores and reported larger
10 summer concentrations attributed to North American biomass burning. However, circulation
11 at the lower latitudes of Canary Island is quite different. Attempts to determine the global FT
12 distribution of NO₂, based on the cloud slicing technique, have recently been made with OMI
13 data (Choi et al, 2014), but the method does not provide results in summer over the Sahara
14 region due to lack of cloudiness.

15 HYSPLIT 7 days back trajectory cluster analysis shows that airmasses arriving to Izaña
16 during the reporting period are fundamentally of Atlantic origin, with a small portion arriving
17 from Africa during the summer period (Fig. 6), in agreement with the 22-year (1988-2009)
18 backward trajectory climatology reported by Cuevas et al. (2013). As previously mentioned,
19 only NO₂ observations under no-dust conditions are considered, therefore days with African
20 trajectories are not included in the analysis. Winter trajectories are longer than the summer
21 ones and 30% of them cross the United States. All trajectory clusters show a steady
22 descendent transport in the last 96 hours prior to the arrival to Izaña and are originated at an
23 altitude of 4000-5500 m a.s.l.

24 The cluster analysis tells us that the origin of the NO₂ seasonal variation has to be searched in
25 the Western Atlantic area at much higher altitude than the station. The CAM-Chem model
26 sampled at the 5.9 km level shows larger summer values over North America and the
27 subtropical Atlantic, than in winter months, both in the range of the observed values (Fig. 7).
28 The phase of the mid-troposphere seasonal wave is opposite of the BL one (Lamsal et al.,
29 2010) and is probably due to a combination of seasonality in convection and lightning. Venting
30 processes from the BL to the FT over US has been studied (i.e. Parrish et al., 2004; Hudman
31 2007) finding export of NO_y, mainly in form of HNO₃ and PAN to the mid troposphere.
32 Convection is driven by surface insolation and has a clear seasonal wave. The same is true for

1 lightning since thunderstorms mainly occur during the spring-summer months.

2 Tropospheric vertical profiles (Fig. 8) show how NO₂ vmr are decreasing in wintertime from
3 the MBL to the mid FT whereas in summer the concentration remains constant up to 6 km
4 and then increases. At the 5 km level, the model shows differences from 15 to 40 pptv from
5 winter to summer. These calculated values are in agreement with the 40-50 pptv background
6 NO₂ vmr estimated by Choi et al., (2014) for the summer months FT in an extended area
7 covering the Western Atlantic from subtropics to mid latitudes.

8 The build-up is basically due to enhanced NO₂ formation via the NO+O₃ reaction under
9 higher concentration of NO as result of NO_y reconversion of PAN and HNO₃ in the FT. Note
10 that the lifetime of NO_y is long enough for NO_x-rich air masses, originated in North America,
11 to reach the African coast.

12 In summary, the NO₂ seasonal variation obtained from MAXDOAS measurements can be
13 explained with the help of the back trajectory cluster analysis and a chemistry-climate model
14 and result from a mixed effect of long-range transport and free tropospheric subsidence. This
15 is basically the same conceptual model that explains the origin or relatively high ozone values
16 recorded at Izaña in summertime described by Cuevas et al. (2013). The origin of the high
17 summer NO₂ values at Izaña is related to the larger background NO₂ vmr found over North
18 America in the mid FT, confirming earlier findings from Schultz et al. (1998).

19

20 **7 Summary**

21 NO₂ volume mixing ratio at the level of the high mountain observatory of Izaña (2370 m
22 a.s.l.) has been obtained for 3 years of data using the MAXDOAS technique and the recently
23 reported Modified Geometrical Approximation (MGA). The method uses the absorption of
24 the O₂-O₂ collisional complex at 477 nm to obtain the horizontal path and is applicable in a
25 near-Rayleigh atmosphere. Only data from airmasses of aerosol optical depths below 0.1 were
26 considered, thus removing African airmasses loaded with Saharan dust. Results show that on
27 most of the observation days, data are representative of the free troposphere. Exceptions are
28 found when wind blows from the South. On these occasions, we find evidence that
29 orographically forced surface airmasses ascend upslope to the Izaña observatory providing a
30 channel for irreversible transport of surface origin species to the free troposphere and might
31 provide an explanation for the concentrations of halogens oxides found in this region.

1 The NO₂ seasonal evolution shows a well defined annual cycle in phase with solar radiation.
2 Mean mixing ratios ranges from 20 pptv in mid winter to 42 pptv in summer with a
3 significant day to day variability. By contrast, we find a small interannual variability during
4 the 3-year observation period. A number of possible causes to explain the observed
5 seasonality have been discussed including seasonal changes in transport and contamination
6 due to seasonality in the upslope winds (anabatic winds) but they individually could not
7 provide an explanation of the observations. CAM-Chem climate chemistry model reproduces
8 the monthly distribution with great accuracy. The results of the back trajectory cluster
9 together with the model analysis show that the seasonality in NO₂ vmr is related to a
10 combined effect of long-range transport and subsidence in the free troposphere. Dust-free
11 trajectories follow North America/North Atlantic pathways with airmasses coming from the
12 mid-free troposphere, between 4000 and 5500 m a.s.l. The model and previous satellite
13 estimations show a seasonality in NO_y and NO₂ in the mid free troposphere in phase with the
14 MAXDOAS observations at Izaña. Larger summer values are probably due to a combination
15 of seasonality in convection and lightning.

16

17 **Acknowledgements**

18 This work was funded by the Spanish National R+D Funding Agency through project
19 AMISOC (CGL2011-24891) and the EU FP7 NORS project (Grant Agreement 284421). The
20 authors gratefully acknowledge NOAA Air Resources Laboratory for the provision of the
21 HYSPLIT transport and dispersion model.

22

23

1 **References**

- 2 Anderson, G. P.: AFGL atmospheric constituent profiles (0-120 km), Hanscom AFB, MA :
3 Optical Physics Division, Air Force Geophysics Laboratory, AFGL-TR ; 86-0110. U.S. Air
4 Force Geophysics Laboratory. Optical Physics Division, 1986.
- 5 Baidar, S., Oetjen, H., Coburn, S., Dix, B., Ortega, I., Sinreich, R., and Volkamer, R.: The
6 CU Airborne MAX-DOAS instrument: vertical profiling of aerosol extinction and trace
7 gases, *Atmos. Meas. Tech.*, 6, 719–739, 2013.
- 8 Barret, B., De Maziere, M. D., and Demoulin, P.: Retrieval and characterization of ozone
9 profiles from solar infrared spectra at the Jung-fraujoch, *J. Geophys. Res.* 107(D24), 4788,
10 doi:10.1029/2001JD001298, 2002.
- 11 Bradshaw, J., Newell, R., Sandholm S., and Liu, S.: Observed distributions of nitrogen oxides
12 in the remote free troposphere from the NASA Global Tropospheric Experiment Programs,
13 *R. Geophysics*, 38, 1, 2000.
- 14 Bucselá, E. J., Perring, A. E., Cohen, R. C. Boersma, K. F., Celarier, E. A. Gleason, J. F.,
15 Wenig, M. O., Bertram, T. H., Wooldridge, P.J., Dirksen, R., and Veefkind, J. P.:
16 Comparison of tropospheric NO₂ from in situ aircraft measurements with near-real-time
17 and standard product data from OMI, *J. Geophys. Res.*, V 113, D16S31,
18 doi:10.1029/2007JD008838, 2008.
- 19 Carroll, M.A., Hastie, D.R., Ridley, B.A., Rodgers, M. O., Torres, A. L., Davis, D. D.,
20 Bradshaw, J. D. Sandholm, S. T., Schiff, H.I., Karecki, D. R., Harris, G. W. Mackay, G. I.,
21 Gregory, G. L., Condin, E. P., Trainer, M., Hübler, G., Montzka, D. D., Madronic, S., H.,
22 Albritton, D. L., Singh, H. B., Beck, S. M., Shipham, M.C. and Bachmeier, A. S. Aircraft
23 Measurements of NO_x over the Eastern Pacific and Continental United States and
24 Implications for Ozone Production, *J. Geophys. Res.* V95, D7, pp 10.205-10.233, 1990.
- 25 Chipperfield, M. P.: New version of the TOMCAT/SLIMCAT off-line chemical transport
26 model: Intercomparison of stratospheric tracer experiments, *Q. J. R. Meteorol. Soc.*, 132,
27 1179–1203, doi:10.1256/qj.05.51, 2006.
- 28 Choi, S., Joiner, J., Choi, Y., Duncan, B. N., Vasilkov, A., Krotkov, N., and Bucselá, E.: First
29 estimates of global free tropospheric NO₂ abundances derived using a cloud slicing

1 technique applied to satellite observations from the Aura Ozone Monitoring Instrument
2 (OMI), *Atmos. Chem. Phys.*, 14, 10565–10588, doi:10.5194/acp-14-10565-2014, 2014.

3 Clémer, K., Van Roozendael, M., Fayt, C., Hendrick, F., Hermans, C., Pinardi, G., Spurr, R.,
4 Wang, P., and De Mazière, M., Multiple wavelength retrieval of tropospheric aerosol
5 optical properties from MAXDOAS Measurements in Beijing, *Atmos. Meas. Tech.*, 3,
6 863–878, doi:10.5194/amt-3-863-2010, 2010.

7 Cuevas, E., González, Y., Rodríguez, S., Guerra, J. C., Gómez-Peláez, A. J., Alonso-Pérez,
8 S., Bustos, J., and Milford, C., Assessment of atmospheric processes driving ozone
9 variations in the subtropical North Atlantic free troposphere, *Atmos. Chem. Phys.*, 13,
10 1973-1998, doi:10.5194/acp-13-1973-2013, 2013.

11 Cuevas, C., Notario, A., Adame, J.A., Hilboll, A., Richter, A., Burrows, J. P. and A. Saiz-
12 Lopez, Evolution of NO₂ levels in Spain from 1996 to 2012, *Scientific Reports*, 4, 5887;
13 DOI:10.1038/srep05887, 2014.

14 Denis, L., Roscoe, H. K., Chipperfield, M. P., Van Roozendael, M., and Goutail, F.: A new
15 software suite for NO₂ vertical profile retrieval from ground-based zenith-sky
16 spectrometers, *J. Quant. Spectrosc. Rad. Transf.*, 92, 321–333,
17 doi:10.1016/j.jqsrt.2004.07.030, 2005.

18 Draxler, R.R., Stunder, B., Rolph, G., Taylor, A. 2009. HYSPLIT_4 User's Guide, via NOAA
19 ARL website. NOAA Air Resources Laboratory, Silver Spring, MD, December 1997 (last
20 access: May 19, 2015), revised January 2009.
21 http://www.arl.noaa.gov/documents/reports/hysplit_user_guide.pdf

22 Emmons, L. K., Walters, S., Hess, P. G., Lamarque, J.-F., Pfister, G. G., Fillmore, D.,
23 Granier, C., Guenther, A., Kinnison, D., Laepple, T., Orlando, J., Tie, X., Tyndall, G.,
24 Wiedinmyer, C., Baughcum, S. L. and Kloster, S.: Description and evaluation of the Model
25 for Ozone and Related chemical Tracers, version 4 (MOZART-4), *Geosci. Model Dev.*,
26 3(1), 43–67, doi:10.5194/gmd-3-43-2010, 2010.

27 Fernandez, R. P., Salawitch, R. J., Kinnison, D. E., Lamarque, J.-F. and Saiz-Lopez, A.:
28 Bromine partitioning in the tropical tropopause layer: implications for stratospheric
29 injection, *Atmos. Chem. Phys.*, 14, 13391-13410, doi:10.5194/acp-14-13391-2014, 2014.

30 Flynn, C. M., Pickering, K. E., Crawford, J. H., Lamsal, L. N., Krotkov, N. A., Herman, J.,
31 Weinheimer, A., Chen, G., Liu, X., Szykman, J., Tsay, S. C., Laughner, C. P., Hains, J.,

1 Lee, P., Dickerson, R. R., Stehr, J. W., and Brent, L.: The relationship between column-
2 density and 20 surface mixing ratio: statistical analysis. *Atmos. Environ.* 92, 429-441,
3 2014.

4 Friess, U., Monks, P. S., Remedios, J. J., Rozanov, A., Sinreich, R., Wagner, T., and Platt, U.:
5 MAX-DOAS O₄ measurements: A new technique to derive information on atmospheric
6 aerosols: 2. Modeling studies, *J. Geophys. Res.*, 111, D14203, doi:10.1029/2005JD006618,
7 2006.

8 Gómez, L., Navarro-Comas, M., Puente-dura, O., Gonzalez, Y., Cuevas, E. and Gil-Ojeda, M.:
9 Long-path averaged mixing ratios of O₃ and NO₂ in the free troposphere from mountain
10 MAX-DOAS *Atmos. Meas. Tech.*, 7, 1-12, 2014.

11 Granier, C., Guenther, A., Lamarque, J. F., Mieville, A., Muller, J., Olivier, J., Orlando, J.,
12 Peters, J., Petron, G., Tyndall, G., and Wallens, S.: POET, a database of surface emissions
13 of ozone precursors, available at at: <http://www.aero.jussieu.fr/projet/ACCENT/POET.php>
14 (last access: May 19, 2015), 2005.

15 Heland, J., Schlanger, H., Richter A., and Burrows, J.P.: First comparison of tropospheric
16 NO₂ column densities retrieved from GOME measurements and in situ aircraft profile
17 measurements, *Geophys. Res. Lett.*, V29, N20, 1983, doi:10.1029/2002GL015528, 2002.

18 Hermans C., O₄ absorption cross-sections at 298K (335.59-666.63 nm), available at:
19 <http://spectrolab.aeronomie.be/index.htm> (last access: May 19, 2015), 2011.

20 Hilboll, A., Richter A., and Burrows, J. P.: Long-Term changes of tropospheric NO₂ over
21 megacities derived from multiple satellite instruments, *Atmos. Chem. Phys.*, 13, 4145–
22 4169, 2013.

23 Hudman, R. C., Jacob, D. J., Turquety, S., Leibensperger, E. M., Murray, L. T., Wu, S.,
24 Gilliland, A. B., Avery, M., Bertram, T. H., Brune, W., Cohen, R. C., Dibb, J. E., Flocke,
25 F. M., Fried, A., Holloway, J, Neuman, J. A., Orville, R., Perring, A., Ren, X., Sachse, G.
26 W., Singh, H. B., Swanson A., and Wooldridge, P. J.: Surface and lightning sources of
27 nitrogen oxides over the United States: Magnitudes, chemical evolution, and outflow, *J.*
28 *Geophys. Res.*, 112, D12S05, doi:10.1029/2006JD007912, 2007.

29 Irie, H., Sudo, K., Akimoto, H., Richter, A. Burrows, J. P., Wagner, T., Wenig, M., Beirle, S.
30 Kondo, Y., Sinyakov V. P. and Goutail, F.: Evaluation of long-term tropospheric NO₂ data

1 obtained by GOME over East Asia in 1996-2002, *Geophys. Res. Lett.*, V32, L11810,
2 doi:10.1029/2005GL022770, 2005.

3 Jacob, D.J., Crawford, J. H., Kleb, M- M., Connors, V. S., Bendura, R. J., Raper, J. L.,
4 Sachse, G. W., Gille, J. G., Emmons, L., and Heald, C. L.: Transport and Chemical
5 Evolution over the Pacific (TRACE-P) aircraft mission: Design, execution, and first
6 results, *J. Geophys. Res.*, V 108, NO. D20, 9000, doi:10.1029/2002JD003276, 2003.

7 Kleissl, J. K., Honrath, R. E., Dziobak, M. P., Tanner, D., Val Martín, M., Owen, R. C. and
8 Helmig, C.: The occurrence of upslope flows at the Pico mountain top observatory: A case
9 study of orographic flows on a small, volcanic island, *J. Geophys. Res.*, 112, D10S35,
10 doi:10.1029/2006JD007565, 2007.

11 Lamarque, J.-F., Emmons, L. K., Hess, P. G., Kinnison, D. E., Tilmes, S., Vitt, F., Heald, C.
12 L., Holland, E. A., Lauritzen, P. H., Neu, J., Orlando, J. J., Rasch, P. J. and Tyndall, G. K.:
13 CAM-chem: description and evaluation of interactive atmospheric chemistry in the
14 Community Earth System Model, *Geosci. Model Dev.*, 5(2), 369–411, doi:10.5194/gmd-5-
15 369-2012, 2012.

16 Lamsal R. N., Martin, R. V., van Donkelaar, A., Celarier, E. A., Bucsela, E. J., Boersma, K.
17 F., Dirksen, R., Luo, C. and Wang, Y.: Indirect validation of tropospheric nitrogen dioxide
18 retrieved from the OMI satellite instrument: Insight into the seasonal variation of nitrogen
19 oxides at northern midlatitudes. *J. of Geophys. Res.*, V. 115, D05302,
20 doi:10.1029/2009JD013351, 2010.

21 Mayer, B. and Kylling, A.: Technical note: The LibRadtran software package for radiative
22 transfer calculations – description and examples of use, *Atmos. Chem. Phys.*, 5, 1855–
23 1877, doi:10.5194/acp-5-1855-2005, 2005.

24 Ordóñez, C., Lamarque, J.-F., Tilmes, S., Kinnison, D. E., Atlas, E. L., Blake, D. R., Sousa
25 Santos, G., Brasseur, G. and Saiz-Lopez, A.: Bromine and iodine chemistry in a global
26 chemistry-climate model: description and evaluation of very short-lived oceanic sources,
27 *Atmos. Chem. Phys.*, 12(3), 1423–1447, doi:10.5194/acp-12-1423-2012, 2012.

28 Parrish D. D., Ryerson, T. B., Holloway, J. S., Neuman, J. A., Roberts, J. M., Williams, J.,
29 Stroud, C. A., Frost, G. J., Trainer, M., Hübler, G., Fehsenfeld, F. C., Flocke F., and
30 Weinheimer, A. J.: Fraction and composition of NO_y transported in air masses lofted from

- 1 the North American continental boundary layer, *J. Geophys. Res.*, V109, D09302,
2 DOI: 10.1029/2003JD004226, 2004.
- 3 Parrish D. D., Ryerson, T. B., Holloway, J. S., Neuman, J. A., Roberts, J. M., Williams, J.,
4 Stroud, C. A., Frost, G. J., Trainer, M., Hübler, G., Fehsenfeld, F. C., Flocke F., and
5 Weinheimer, A. J.: Fraction and composition of NO_y transported in air masses lofted from
6 the North American continental boundary layer, *J. Geophys. Res.*
7 DOI: 10.1029/2003JD004226, 2004.
- 8 Persson, A. and Grazzini, F., User Guide to ECMWF forecast products, *Meteorological*
9 *Bulletin M3.2*, Edited by ECMWF. Available at:
10 [http://www.uio.no/studier/emner/matnat/geofag/GEF4220/v09/undervisningsmateriale/Pers](http://www.uio.no/studier/emner/matnat/geofag/GEF4220/v09/undervisningsmateriale/Persson_user_guide.pdf)
11 [sson_user_guide.pdf](http://www.uio.no/studier/emner/matnat/geofag/GEF4220/v09/undervisningsmateriale/Persson_user_guide.pdf) (last access May 19, 2015), Updated 2007.
- 12 Puentedura, O., Gil, M., Saiz-Lopez, A., Hay, T., Navarro-Comas, M., Gomez-Pelaez, A.,
13 Cuevas, E., Iglesias J., and Gomez, L.: Iodine monoxide in the North subtropical free
14 troposphere, *Atmos. Chem. Phys.*, 12, 4909–4921, doi:10.5194/acp-12-4909-2012, 2012.
- 15 Qi, Y.: Spatio-Temporal distributions of tropospheric NO₂ over Oases in Taklimakan Desert,
16 China, *Chin. Geogra. Sci.*, 1-8, doi:10.1007/s11769-014-0696-z, 2014.
- 17 Reidmiller D.R., Jaffee, D. A., Fischer E. V., and Finley, B.: Nitrogen oxides in the boundary
18 layer and free troposphere at the Mt. Bachelor Observatory, *Atmos. Chem Phys.*, 10, 6043-
19 6062, 2010.
- 20 Richter, A., Burrows, J. P., Nüs, H., Granier C., and Niemeier, U.: Increase in tropospheric
21 nitrogen dioxide over China observed from space, *Nature* 437, 129-132,
22 doi:10.1038/nature04092, 2005.
- 23 Ridley, B. A., Carroll, M. A., Gregory, G. L., and Sachse, G. W.: NO and NO₂ in the
24 troposphere: Technique and measurements in regions of a folded tropopause *J. Geophys.*
25 *Res.*, 93, 15,813-15,830, 1988.
- 26 Rodgers, C. D.: *Inverse Methods for Atmospheric Sounding: Theory and Practice*, vol. 2 of
27 *Atmospheric, Oceanic and Planetary Physics*, World Scientific, Hackensack, NJ,
28 doi:10.1142/9789812813718_fmatter, 2000.
- 29 Rodriguez, S., Y. Gonzalez, E. Cuevas, R. Ramos, P. M. Romero, J. Abreu-Afonso and A.
30 Redondas, Atmospheric nanoparticle observations in the low free troposphere during

1 upward orographic flows at Izana Mountain Observatory *Atmos. Chem. Phys.*, 9, 6319–
2 6335, 2009.

3 Saiz-Lopez, A., Lamarque, J.-F., Kinnison, D. E., Tilmes, S., Ordóñez, C., Orlando, J. J.,
4 Conley, A. J., Plane, J. M. C., Mahajan, A. S., Sousa Santos, G., Atlas, E. L., Blake, D. R.,
5 Sander, S. P., Schauffler, S., Thompson, A. M. and Brasseur, G.: Estimating the climate
6 significance of halogen-driven ozone loss in the tropical marine troposphere, *Atmos.*
7 *Chem. Phys.*, 12(9), 3939–3949, doi:10.5194/acp-12-3939-2012, 2012.

8 Chipperfield, M. P.: New version of the TOMCAT/SLIMCAT off-line chemical transport
9 model: Intercomparison of stratospheric tracer experiments, *Q. J. R. Meteorol. Soc.*, 132,
10 1179–1203, doi:10.1256/qj.05.51, 2006.

11 Schultz, M., Schmitt, R., Thomas, K., Volz-Thomas, A., Photochemical box modeling of
12 long-range transport from North America to Tenerife during the North Atlantic Regional
13 Experiment (NARE) 1993, *J. Geophys. Res.* 103, D11, 13477–13488, DOI:
14 10.1029/97JD01481, 1998.

15 Spinei, E., Cede, A., Herman, J., Mount, G. H., Eloranta, E., Morley, B., Baidar, S., Dix, B.,
16 Ortega, I., Koenig, T. and Volkamer, R.: Direct sun and airborne MAX-DOAS
17 measurements of the collision induced oxygen complex, O₂O₂ absorption with significant
18 pressure and temperature differences, *Atmos. Meas. Tech. Discuss.*, 7, 10015-10057, 2014.

19 Stunder, B. An assessment of the Quality of Forecast Trajectories. *Journal of Applied*
20 *Meteorology* 35, 1319-1331, 1996.

21 Thalman, R., and Volkamer, R. Temperature dependent absorption cross-sections of O₂-O₂
22 collision pairs between 340 and 630 nm and at atmospherically relevant pressure, *Phys*
23 *Chem Chem Phys.*, 15, doi: 10.1039/c3cp50968k, 2013.

24 Vandaele, A. C., Hermans, C., Simon, P. C., Carleer, M., Colins, R., Fally, S., Mérienne, M.
25 F., Jenouvrier, A., and Coquart, B.: Measurements of the NO₂ Absorption Cross-Sections
26 from 42000 cm⁻¹ to 10000 cm⁻¹ (238–1000 nm) at 220 K and 294 K, *J. Quant. Spectrosc.*
27 *Ra.*, 59, 171–184, doi:10.1016/S0022-4073(97)00168-4, 1998.

28 Val-Martin, M., Honrath, R. E., Owen, R. C., and Li, Q. B.: Seasonal variation of nitrogen
29 oxides in the central North Atlantic lower free troposphere *J. Geophys. Res.*, V113,
30 D17307, doi:10.1029/2007JD009688, 2008.

- 1 Van der A., R. J., Peters, D. H. M. U., Eskes, H., Boersma, K. F., Van Roozendaal, M., De
2 Smedt, I., and Kelder, H. M.: Detection of the trend and seasonal variation in tropospheric
3 NO₂ over China, *J. of Geophys. Res.*, V111, D12317, doi:10.1029/2005JD006594, 2006.
- 4 Wagner, T., Dix, B., Friedeburg, C.V., Friess, U., Sinreich, R., and Platt, U.: MAX-DOAS O4
5 measurements: A new technique to derive information on atmospheric aerosols –
6 Principles and information content, *J. Geophys. Res.*, 109, D22205, doi:10-
7 1029/2004JD0044904, 2004.
- 8 Wagner, T., von Friedeburg, C., Wening, M., Otten, C., and Platt, U.: UV-Visible
9 observations of atmospheric O4 absorptions using direct moonlight and zenith-scattered
10 sunlight for clear sky and cloudy sky conditions, *J. Geophys. Res.*, 107, 4424,
11 doi:10.1029/2001JD001026, 2002.
- 12 Wenger, R. Zur Theorie der Berg- und Talwinde', *Meteorol. Zeits.* 7, 193–204, 1923.
- 13 Wittrock, F., Oetjen, H., Richter, A., Fietkau, S., Medeke, T., Rozanov, A., and Burrows, J.
14 P.: MAX-DOAS measurements of atmospheric trace gases in Ny-Alesund – Radiative
15 transfer studies and their application, *Atmos. Chem. Phys.*, 4, 955–966, doi:10.5194/acp-
16 4-955-2004, 2004.
- 17 Ziemke, J. R., Chandra, S., and Bhartia, P. K.: “Cloud slicing”: a new technique to derive
18 upper tropospheric ozone from satellite measurements, *J. Geophys. Res.*, 106, 9853–9867,
19 2001.
- 20 Zien, A.W., Reichter, A., Hillboll, A., Blechschmidt A.-M., and Burrows, J. P.: Systematic
21 analysis of tropospheric NO₂ long-range transport events detected in GOME-2 satellite
22 data, *Atmos. Chem Phys.*, 14, 7367-7396, doi:10.5194/acp-14-7367-2014, 2014.
- 23

1
2
3
4
5
6
7
8
9
10
11
12

Table 1. Method uncertainty	
Uncertainty in NO ₂ due to fit	15-20%
Uncertainty in path due to the O ₄ fit	< 1%
Uncertainty of the method (related to unknown vertical distribution of NO ₂ and actual effective path)	2.5-9% (for sza: 50° to 70°)
Error in horizontal path due to O ₄ cross-sections temperature dependence	2%
OVERALL UNCERTAINTY	20-32%

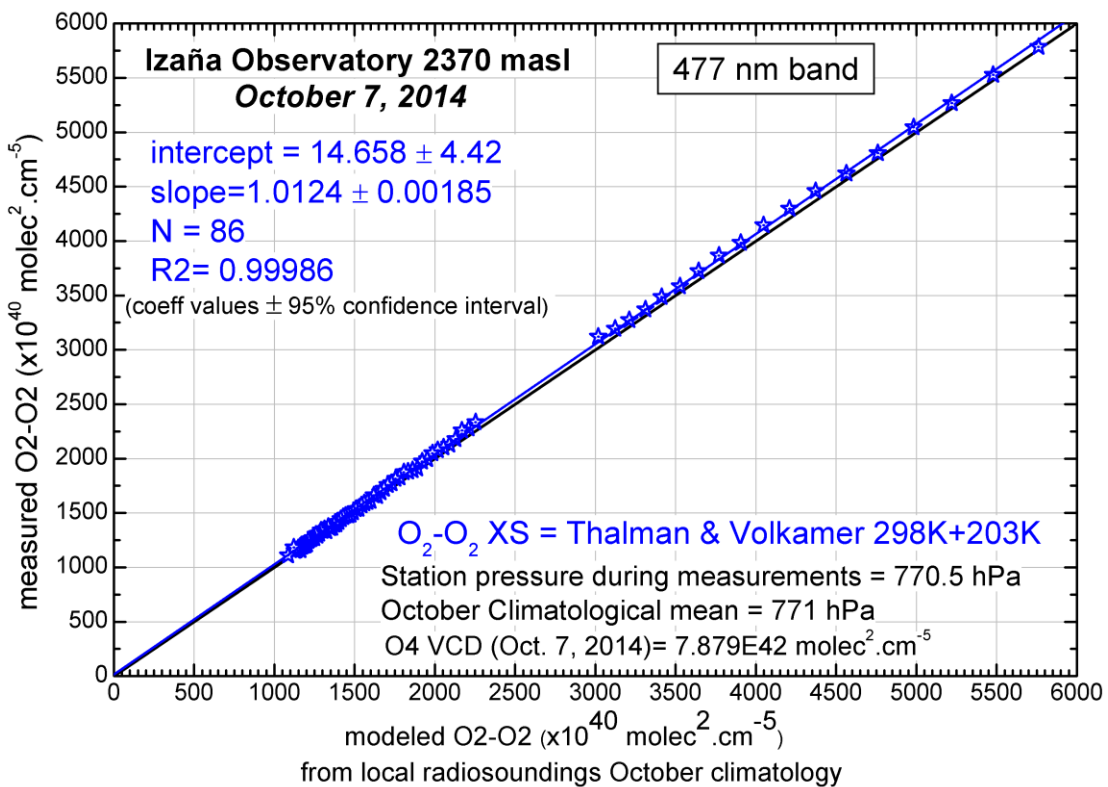
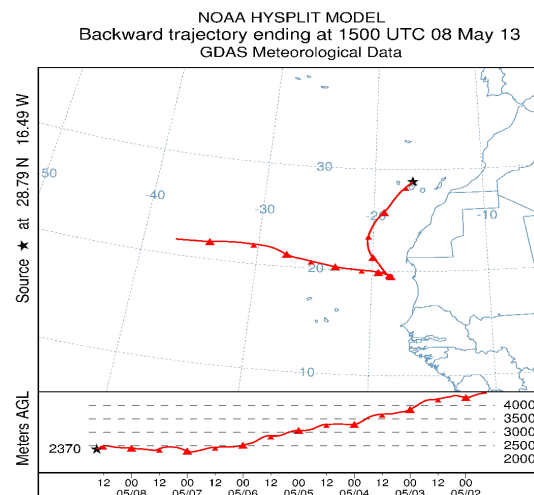
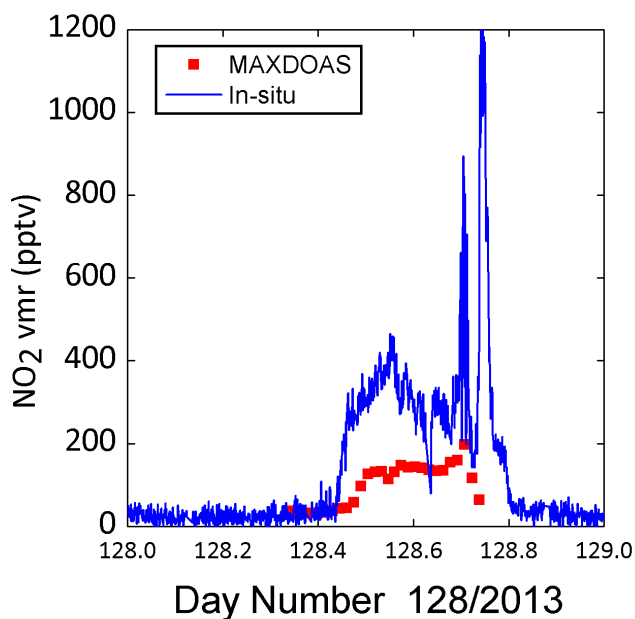
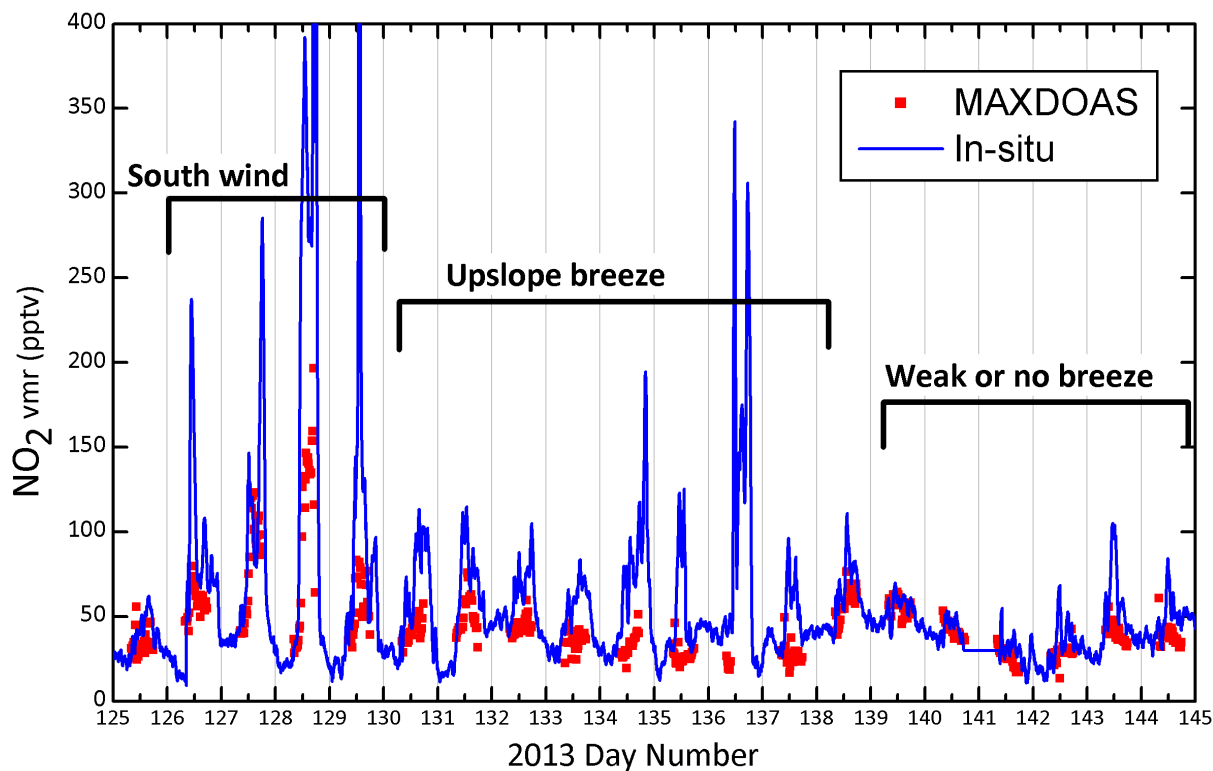
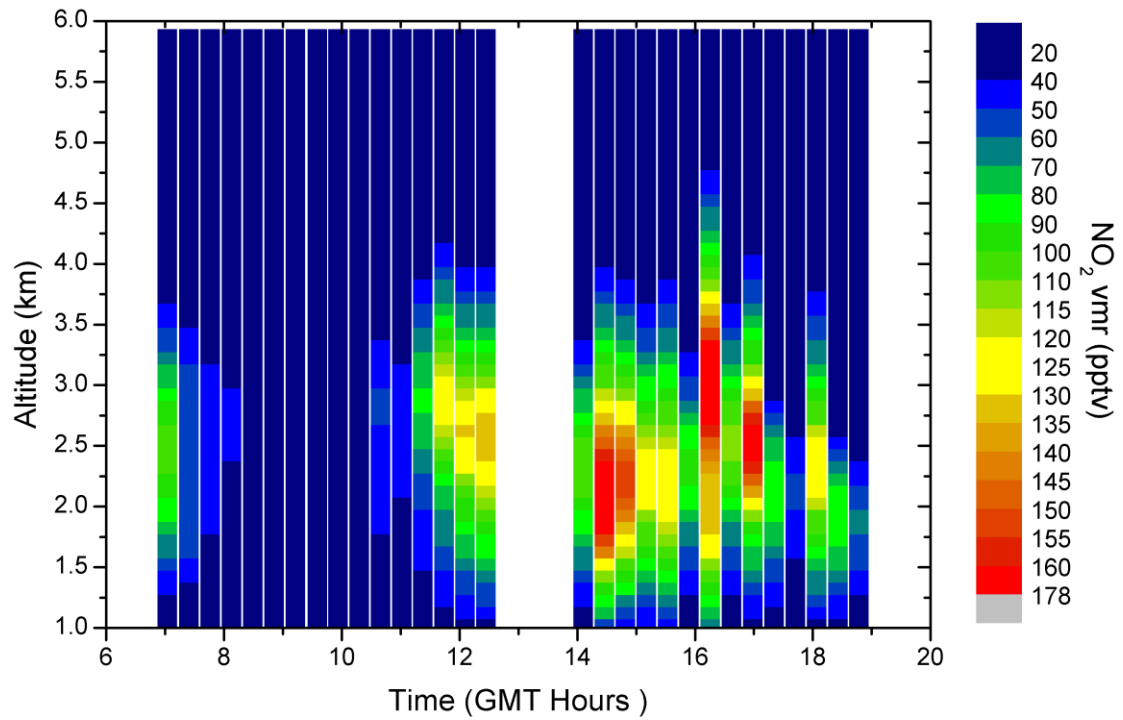


Figure 1. Measured O₄ SCD versus modeled O₄ for a pure Rayleigh atmosphere at the 477 nm band by using cross-sections at 203K and 293K temperatures (see text for details)



1
 2 Figure 2. Izaña MAXDOAS versus minutal in-situ NO₂ volume mixing ratio for a period of
 3 time representative of 3 different wind situation. *In-situ* data are smoothed by 50-minutes
 4 running mean. (Top panel). Expanded plot for day May 8, 2013 (day number 128).
 5 Backtrajectory ending at Izaña at 15h of the same day.

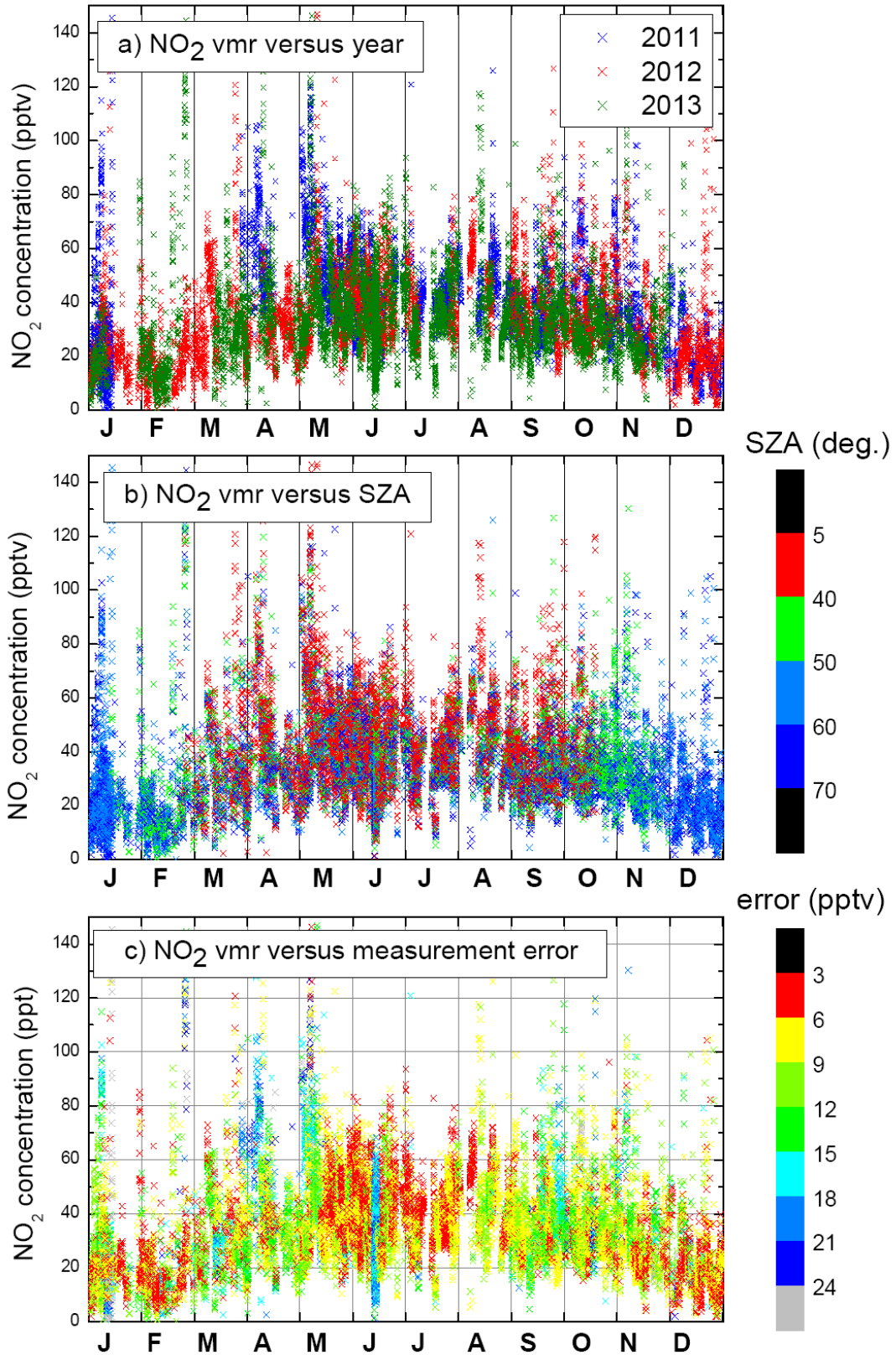
6



1

2 Figure 3. Unsmoothed vertical profiles of NO₂ vmr (in pptv) for day 128/2013 obtained by
 3 OEM technique. Each vertical column represents an individual scanning cycle. (For details
 4 see text)

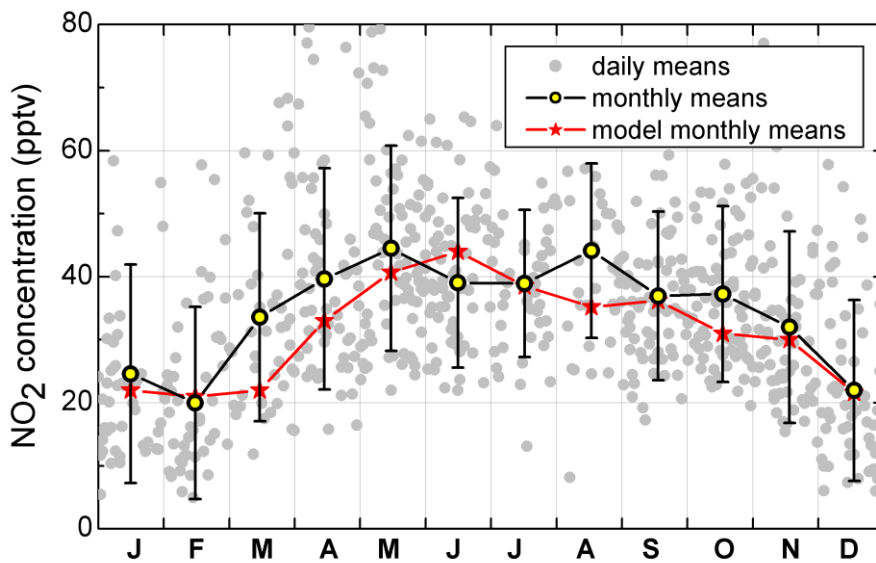
5



2

3 Figure 4. Seasonal evolution of the individual data NO₂ vmr separated by years (Upper
 4 panel). Separated by Solar Zenith Angles (Mid panel) and separated by RMSE (Lower panel).

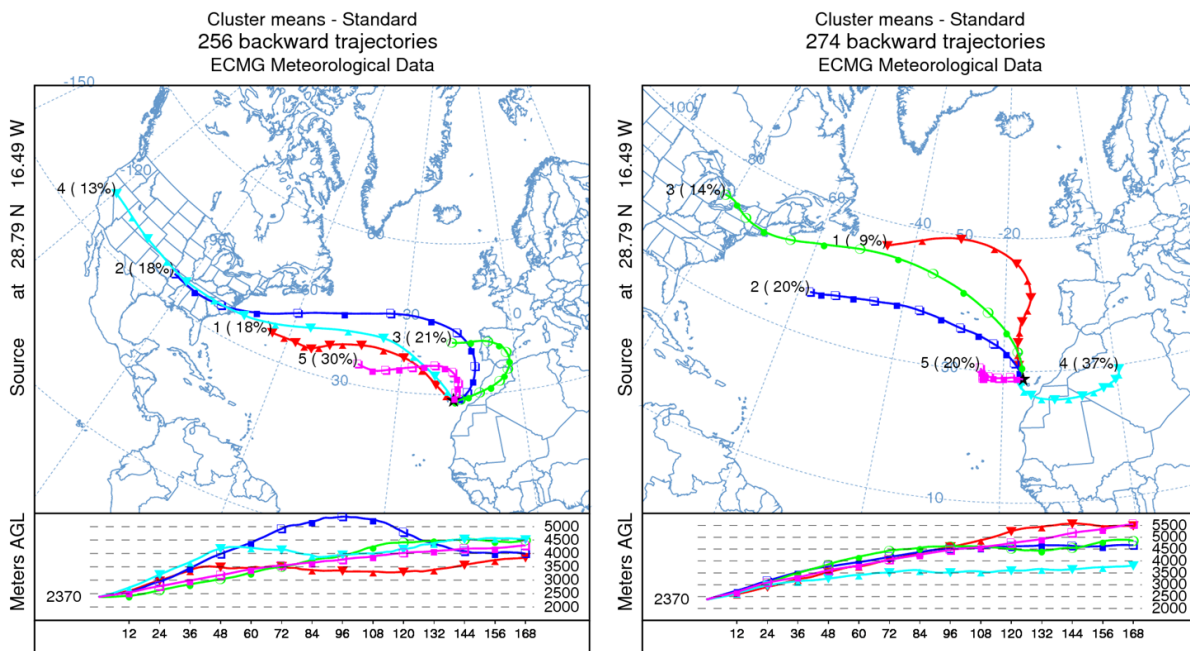
1



2

3 Figure 5. NO₂ concentration monthly means at the level of Izaña Observatory with their
 4 respective standard deviations (open circles and black lines). CAM-Chem model results for
 5 the same level are shown for comparison (Red stars and lines). Individual solid grey circles
 6 are the 3-years diurnal mean

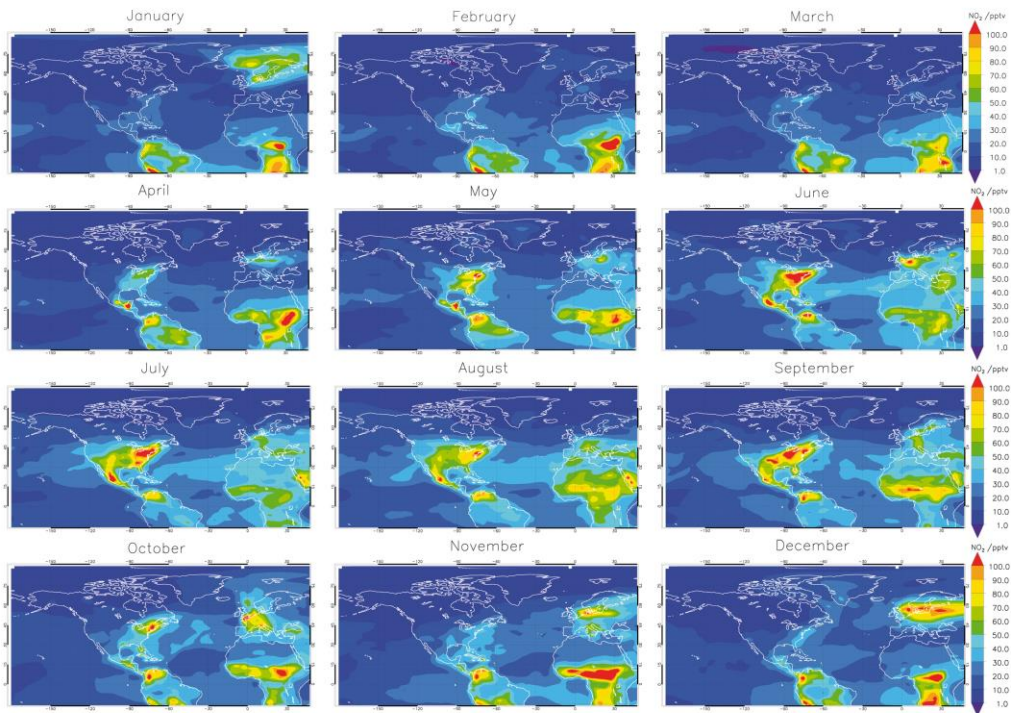
7



8

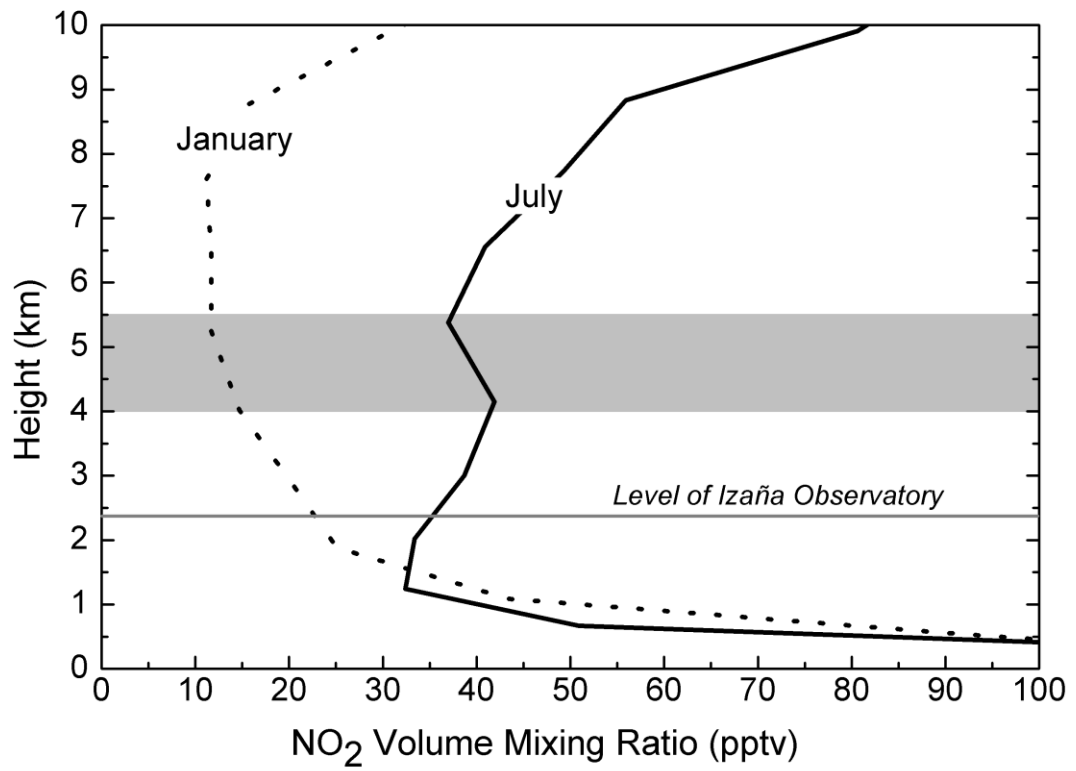
9 Figure 6. 1-week HYSPLIT back trajectories clusters arriving to Izaña Observatory for the
 10 left panel: winter months (DJF), right panel: summer months (JJA) and years 2011-2013

1



2

3 Figure 7. Global distributions of monthly mean NO₂ vmr for the level 5.9 km obtained from
4 the Cam-CHEM chemistry climate model-model.



1

2 Figure 8. NO₂ vmr monthly means vertical profiles from Cam-CHEM model.

3 Gray band represents the height range where airmasses are originated (see text).